Development of a Tilt Control Method for a Narrow Track Three Wheeled Vehicle

Revised Paper Submitted on April 21, 2011

Authors: Dr J. Berote, Dr J. Darling and Prof. A. Plummer

Department of Mechanical Engineering
University of Bath
Bath, BA2 7AY
U.K.

Abstract

The space and weight savings provided by narrow tilting vehicles could make them a solution to the pollution and congestion problems seen in urban environments. The success of this new type of vehicle relies heavily on the control method used to balance the vehicle in corners. A tilting three-wheeled vehicle was developed at the University of Bath as part of an EU funded project. The original direct tilt control method implemented on the prototype was shown to perform well in steady state, but rapid transients were shown to potentially lead to instability. A new type of controller was therefore required to reduce the load transfer across the rear axle during transient state manoeuvres.

This paper presents a linearised model of the tilting vehicle system which is used to optimise a new tilt controller in the frequency domain. The controller, which uses combined steer and tilt control inputs, is shown to significantly reduce transient roll moments compared to the previous control method. This results in a much safer and more predictable handling characteristic.

Key Words: tilt control, handling, narrow track, tilting, three-wheeled vehicle, linearised model, frequency response

1 Introduction

Narrow track vehicles can provide a significant reduction in weight and frontal area compared to ordinary cars. This provides a small road footprint as well as improved fuel efficiency. As EU car manufacturers are committed to reduce their overall fleet emissions to 130g/km by 2015 with a long term target of 95g/km for the year 2020 [1], a small vehicle with emissions equivalent to that of a motorcycle would greatly help the companies to reach these targets. In order for such a vehicle to be as safe as a larger car, it must be relatively tall and fully enclosed. Due to the tall and narrow nature of the vehicle, it will be prone to rolling over during cornering. To prevent this from happening, it is necessary to tilt the vehicle into the turn in order to compensate for the moment caused by the lateral force generated by the tyres.

Most control strategies can be classified as direct-tilt-control (DTC) or steer-tilt-control (STC). With DTC an actuator is used to tilt the vehicle into the corner. In severe manoeuvres this can lead to large transient load transfers onto the outer wheels, which can ultimately lead to the roll-over of the vehicle. In STC the balancing effect is achieved through counter-steer. Although this is favourable in terms of load transfer, this type of system is unstable at lower speeds. Recent work has therefore been focused on combining these two control strategies (dual-control or SDTC) to achieve stability at all vehicle speeds. Early attempts were made by So and Karnopp [2] [3] suggesting a speed dependent strategy and it was found that this system performed poorly at the switching points. A system was then introduced which could switch between the two tilt systems depending on the error between the demand and the output lateral acceleration [4]. It was again recognised that the switching could be improved to obtain a smoother output. These strategies were demonstrated in simulation and experimental data remains scarce.

The work in this paper is based on the CLEVER vehicle [5], a three-wheel prototype vehicle developed at the University of Bath as part of an EU funded project. The current control strategy utilises measurements of speed and steer to predict the lateral acceleration and hence the tilting angle required to balance the vehicle during cornering.

Figure 1: CLEVER test vehicle at the University of Bath

This angle is referred to as the equilibrium or steady state angle, θ_{ss}:

$$\theta_{ss} = tan^{-1}\left(\frac{a_y}{g}\right) \approx \frac{a_y}{g} \tag{1}$$

Assuming that the handling characteristic remains neutral, the steer angle will be close to the Ackerman angle. The cornering radius R can therefore be estimated from the front steer angle δ_f and the wheelbase L as shown in equation 2.

$$\tan\delta_f = \frac{L}{R} \Longrightarrow R = \frac{L}{\tan\delta_f} \tag{2}$$

The lateral acceleration can be estimated from the vehicle forward velocity as shown equation 3.

$$a_y = \omega^2 R = \frac{V^2}{R} \tag{3}$$

Equation 1, 2 and 3 can be combined to estimate the necessary steady state θ_{ss} or demand θ_d tilt angle.

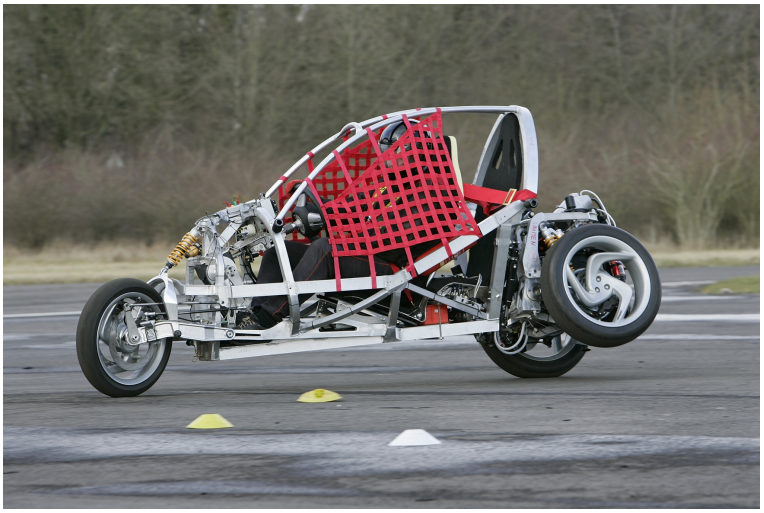

Figure 2: Lifting of inner wheel due to an aggressive steering manoeuvre

$$\theta_{ss} = \theta_d = tan^{-1}\left(\frac{a_y}{g}\right) = tan^{-1}\left(\frac{V^2 \tan\delta_f}{Lg}\right) \approx \frac{V^2\delta_f}{Lg} \tag{4}$$

Equation 4 does not take into account the non-tilting rear module, the height of the tilt-axis above the ground which results in a smaller absolute tilt angle and the tyre slip angles generated at higher lateral accelerations. Furthermore, the equation was linearised for use in the controller as shown by the approximation in equation 4.

The cabin of the vehicle is tilted to the desired angle using two hydraulic actuators. Although the vehicle performs well in steady state, aggressive transient manoeuvres can lead to the roll-over of the vehicle [6], as shown in figure 2.

The CARVER is a production vehicle of similar configuration to CLEVER. The main difference is that the CARVER utilises its Dynamic Vehicle Control (DVC^{TM}) technology to control the tilting and it is also wider (1.3m as opposed to 1m). The tilt control solution is based on a mechanically operated hydraulic system. A hydraulic valve opens according to the amount of steering torque at the front wheel and remains open until the steer torque is zero. The entire system was developed experimentally and is quite mechanically complex. The engineers of Brink Dynamics have published a few papers

on their technology [7] [8] [9]. These, however, do not contain any data on the dynamic performance of the vehicle. Another narrow tilting vehicle prototype with four wheels arranged in a diamond shape was recently developed and constructed at the National Chiao Tung University in Taiwan. The dual-tilt control strategy using a double-loop PID Controller is presented by Chiou et al. [10] [11].

The system proposed here combines both steer and tilt control concurrently, using the driver steering input and vehicle speed as the only input parameters. Recently, a similar combined system was presented by Kidane et al. [12] [13], together with experimental results. However, these were limited to time domain plots of standard manoeuvres at low frequencies. This paper presents a linearised model which is tested against a non-linear multi-body model of the vehicle [14]. This allows a comparison of a DTC system and the proposed STDC control method in the frequency domain. The resultant lateral acceleration and load transfer response for both control methods are compared and finally the proposed control method is optimised in the frequency domain.

2 Proposed Controller

It has been shown that in order to optimise the lateral dynamics response of the vehicle, independent control of the lateral acceleration through active steer is necessary [15]. This can be achieved by cutting the direct link between the driver steering input and the steering angle at the front wheel. Instead, the driver steering input can be regarded as a lateral acceleration demand, with a controller regulating the tilt angle demand and the steer angle of the front wheel.

If independent control of the steering angle is possible, using a negative gain feedback between the tilt-error and the steer input reduces the amount of steering at the front wheel in proportion to the tilt error. The block diagram shown in figure 3 shows how the front wheel steering angle δ_f and the hydraulic valve displacement x_v are derived. The steering wheel angle δ_w and velocity V are used to calculate the demand lateral acceleration a_{yd}, from which the steady state or demand steer angle δ_d and tilt angle

angle θ_d are obtained. The tilt error θ_e is given by the diffence between the demand tilt angle and actual tilt angle θ. The error is multiplied by steering gain $K_{\delta\theta}$ and subtracted from from demand steer angle to give the applied front wheel steer angle δ_f. The tilt error is also multiplied by the spool displacement gain K_{xv} to give the applied valve spool displacement to direct flow to the hydraulic actuators. The intention is to reduce front wheel steer during aggressive manoeuvres such that the system can reach the desired tilt angle without excessive later forces acting on the vehicle. It will be shown that the controller can lead to some counter-steer under certain circumstances in order to reach the required tilt angle more rapidly.

With the steering gain $K_{\delta\theta}$ set to zero, the controller is analogous to the original CLEVER DTC set-up. The lateral acceleration demand a_{yd} is equivalent to the lateral acceleration estimate of the original controller:

$$a_{yd} = \frac{\delta_w R_w V^2}{L} \tag{5}$$

where δ_w is the driver input at the steering wheel, R_w is the steering ratio, L is the wheel-base and V is the vehicle forward velocity. Based on the same principle, the steering demand angle δ_d and tilt demand angle θ_d are given by:

$$\delta_d = \frac{a_{yd} L}{V^2} \qquad \theta_d = K_\theta \frac{a_{yd}}{g} \tag{6}$$

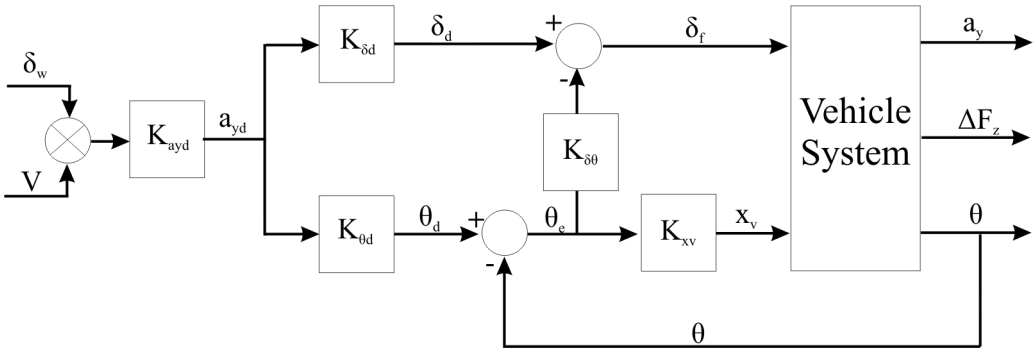

Figure 3: Block diagram for proposed control system

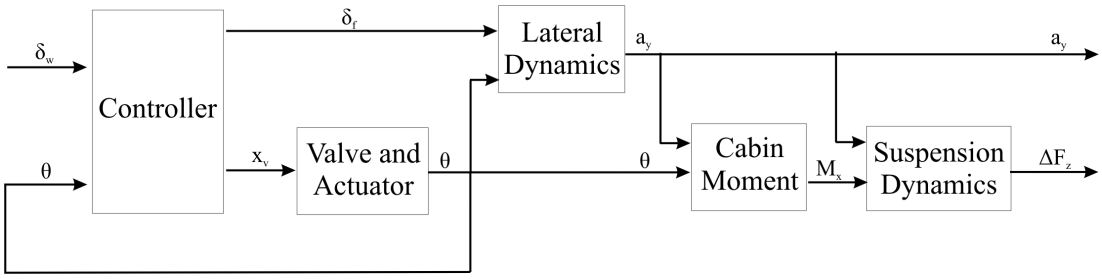

Figure 4: Schematic diagram showing individual blocks required for the linearisation of the vehicle system

where K_θ is a gain that is applied to compensate for the raised tilt axis.

3 Linear Model Derivation

In order to tune the new control approach and assess it against the original controller, a linearised model of the vehicle system was developed. This allowed a quantitative comparison of the old and new system performance in the frequency domain. The two variables that can be controlled are the front wheel steer δ_f, and cabin tilt angle θ. The parameters that affect the handling and stability of the vehicle, and that need to be controlled, are the vehicle lateral acceleration a_y and the load transfer across the rear axle ΔF_z. Therefore a system of transfer functions will be derived to relate the steer and tilt angle demand to the vehicle lateral acceleration and rear axle load transfer. The linearisation process will be split up in order to obtain individual linear models for the vehicle's lateral dynamics (section 3.1), kinematics and resultant cabin moment (section 3.2), suspension dynamics (section 3.3) and dynamics of the valve and actuator system (section 3.4), as represented in the schematic diagram shown in figure 4. These will then be combined as a single transfer function relating the input to the output parameters. The system performance will be analysed over the range 0.01 - 10 Hz, although the principal frequencies of interest are regarded as 0.1 - 2Hz as this encompasses frequencies encountered at the driver/system interface.

3.1 Lateral Motion Dynamics

Using a bicycle model such as the one shown in figure 5, the lateral motion of the vehicle can be described using the equations 7 to 10, where α_f and α_r are the front and rear slip angles. The front wheel camber is equivalent to the tilt angle θ. The front and rear tyre slip stiffnesses and the front tyre camber stiffness are given by $C_{\alpha f}$, $C_{\alpha r}$ and $C_{\theta f}$ respectively. The distance from the vehicle centre of gravity to the front and rear wheels is denoted by a and b as shown in figure 5. The vehicle has a total mass m and yaw inertia I_z.

$$ma_y = C_{\alpha f}\alpha_f + C_{\theta f}\theta + 2C_{\alpha r}\alpha_r \tag{7}$$

$$I_z\ddot{\psi} = aC_{\alpha f}\alpha_f + aC_{\theta f}\theta - 2bC_{\alpha r}\alpha_r \tag{8}$$

$$\alpha_f = \delta_f - \tan^{-1}\left(\frac{\dot{y} + a\dot{\psi}}{\dot{x}}\right) \tag{9}$$

$$\alpha_r = \delta_r - \tan^{-1}\left(\frac{\dot{y} - b\dot{\psi}}{\dot{x}}\right) \tag{10}$$

By substituting for the front and rear slip angles, the linearised equations 11 and 12 are obtained. The vehicle has a lateral velocity component v and a yaw rate r. The rear steer δ_r is given by the product of the tilt angle θ and the rear steer coefficient $K_{\delta r}$ [16].

$$m(\dot{v} + Vr) = C_{\alpha f}\left(\delta_f - \frac{v + ar}{V}\right) + C_{\theta f}\theta + 2C_{\alpha r}\left(K_{\delta r}\theta - \frac{v - br}{V}\right) \tag{11}$$

$$I_z\dot{r} = aC_{\alpha f}\left(\delta_f - \frac{v + ar}{V}\right) + aC_{\theta f}\theta - 2bC_{\alpha r}\left(K_{\delta r}\theta - \frac{v - br}{V}\right) \tag{12}$$

These can be written in state-space notation with the state vector x and input vector u:

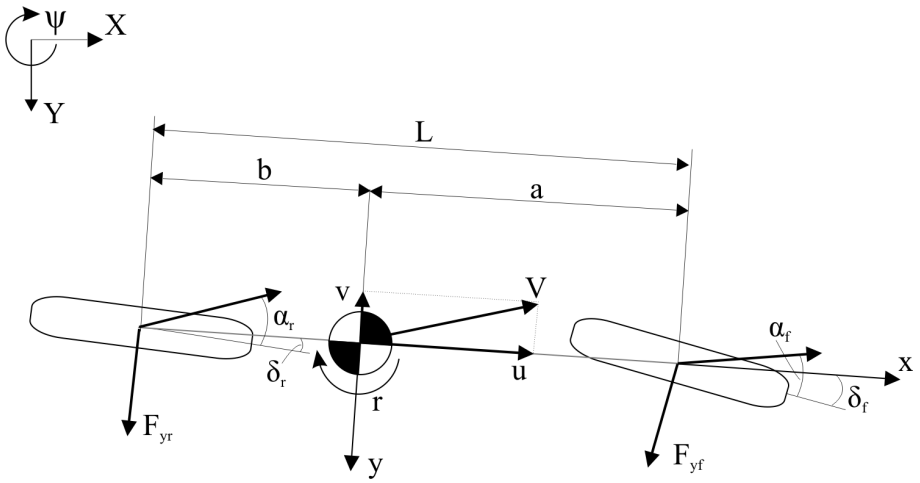

Figure 5: Bicycle model

$$x = \begin{bmatrix} v \\ r \end{bmatrix} \qquad u = \begin{bmatrix} \delta_f \\ \theta \end{bmatrix} \tag{13}$$

V is the forward velocity about which the system is linearised. The output variable y is the lateral acceleration $a_y = (\dot{v} + Vr)$. The A, B, C and D matrices in the standard state space notation are then given by:

$$A = -\begin{bmatrix} \frac{C_{\alpha f}+2C_{\alpha r}}{mV} & V + \frac{C_{\alpha f}a-2C_{\alpha r}b}{mV} \\ \frac{C_{\alpha f}a-2C_{\alpha r}b}{VI_z} & \frac{C_{\alpha f}a^2+2C_{\alpha r}b^2}{VI_z} \end{bmatrix} \qquad B = \begin{bmatrix} \frac{C_{\alpha f}}{m} & \frac{C_{\theta f}a+2C_{\alpha r}K_{\delta_r}}{m} \\ \frac{aC_{\alpha f}}{I_z} & \frac{aC_{\theta f}-2bC_{\alpha r}K_{\delta r}}{I_z} \end{bmatrix}$$

$$C = -\begin{bmatrix} \frac{C_{\alpha f}+2C_{\alpha r}}{mV} & \frac{C_{\alpha f}a-2C_{\alpha r}b}{mV} \end{bmatrix} \qquad D = \begin{bmatrix} \frac{C_{\alpha f}}{m} & \frac{C_{\theta f}+2C_{\alpha r}K_{\delta r}}{m} \end{bmatrix}$$

As the transient state lateral forces play an important role in this study, tyres with a side force subject to a first order lag were introduced. The relaxation length of a tyre is the distance a wheel has to travel to reach 63 % of the steady state force [17] and is denoted as σ. The relaxation length for the camber thrust has been shown to

be negligible [17] [18]. The slip angles in equations 7 and 8 can be replaced by the transient state side slip angles $\alpha_f^{'}$ and $\alpha_r^{'}$:

$$ma_y = C_{\alpha f}\alpha_f^{'} + C_{\theta f}\theta + 2C_{\alpha r}\alpha_r^{'} \tag{14}$$

$$I_z\ddot{\psi} = aC_{\alpha f}\alpha_f^{'} + aC_{\theta f}\theta - 2bC_{\alpha r}\alpha_r^{'} \tag{15}$$

where:

$$\alpha_f = \frac{\sigma}{V}\dot{\alpha}_f^{'} + \alpha_f^{'} \tag{16}$$

$$\alpha_r = \frac{\sigma}{V}\dot{\alpha}_r^{'} + \alpha_r^{'} \tag{17}$$

The transfer function shown in equation 18 can therefore be applied to represent the tyre lag.

$$\frac{\alpha^{'}}{\alpha} = \frac{\frac{V}{\sigma}}{s + \frac{V}{\sigma}} \tag{18}$$

This results in the third order transfer functions G_1 and G_2 describing the relationship between the lateral acceleration and the steer and the lateral acceleration and tilt angle respectively:

$$a_y = G_1\delta_f + G_2\theta \tag{19}$$

3.2 Kinematics and Cabin Moment

The following section derives the actuator moment M_x acting about the tilt bearing based on the vehicle tilt angle θ and the lateral acceleration a_y as shown in figure 4. A free-body diagram of the cabin and rear module is shown in figure 6. The distance

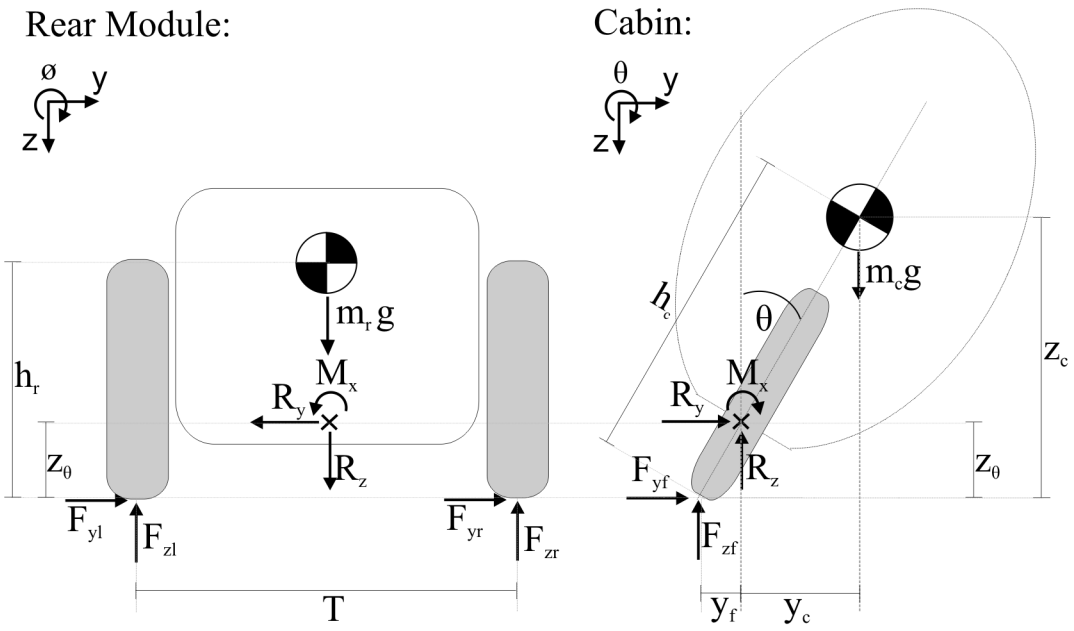

Figure 6: Free body diagram of cabin and rear module viewed from the rear

of the rear module and cabin CoG from the tyre contact point are denoted by h_r and h_c. The vertical distance from the cabin CoG and the tilt bearing from the ground are given by z_c and z_θ. The horizontal distance from the front tyre contact point to the tilt bearing and to the cabin CoG is given by y_f and y_c respectively.

Taking moments about the rear module and the cabin centre of gravity results in the following equations of motion:

$$I_r\ddot{\phi} = R_y(h_r - z_\theta) + (F_{zl} - F_{zr})\frac{T}{2} - h_r(F_{yl} + F_{yr}) - M_x \tag{20}$$

$$I_c\ddot{\theta} = M_x + F_{zf}(y_f + y_c) + R_z y_c - F_{yf} z_c - R_y(z_c - z_\theta) \tag{21}$$

I_r and I_c denote the rear module and cabin roll inertia. The forces on the cabin can be resolved to find the reactions at the tilt bearing R_y and R_z. If $\ddot{z} = 0$ and $\ddot{y} = a_y$ then:

$$R_z = m_c g - F_{zf} \tag{22}$$

$$R_y = m_c a_y - F_{yf} \tag{23}$$

If m represents the total vehicle mass $(m_c + m_r)$, the side force at the front (F_{yf}) and at the rear $(F_{yl} + F_{yr})$ are given by:

$$F_{yf} = \frac{b}{L} m a_y = F_{zf} \frac{a_y}{g} \tag{24}$$

$$F_{yl} + F_{yr} = \frac{a}{L} m a_y = (F_{zl} + F_{zr}) \frac{a_y}{g} \tag{25}$$

In order to obtain an accurate value for the moment applied about the tilt bearing, it is necessary to include the kinematic effects resulting from the tilt bearing inclination. This kinematic effect results in a lateral motion of the front wheel as well as a pitch motion of the rear module as the cabin tilts, which in turn leads to a height reduction in the tilt bearing location. Figure 7 (top) shows an annotated side profile of the vehicle showing the position of the cabin centre of gravity. Figure 7 (middle and bottom) show a side view and top view after a positive (right as viewed from rear) rotation θ about the tilt axis when keeping the rear module fixed.

As a result of the tilt-bearing height reduction, there will also be a shift in the position of the cabin and driver CoG. However this will be so small that it can be neglected.

After some manipulation and using small angle approximations, the linearised equations for y_{fc}, y_c, z_c and z_θ are given by:

$$y_f = (h_\theta + \xi l)\theta \tag{26}$$

$$y_c = (h_c - h_\theta - l_c \xi)\theta \tag{27}$$

$$z_c = \left(h_c - h_\theta \frac{a_c}{a_\theta}\right) + h_\theta \frac{a_c}{a_\theta} \tag{28}$$

$$z_\theta = h_\theta \tag{29}$$

Assigning the variables $z_{c\theta} = (z_c - z_\theta)$ and $y_{fc} = (y_f + y_c)$ we can group the a_y and g terms in equation 21 to give the expression:

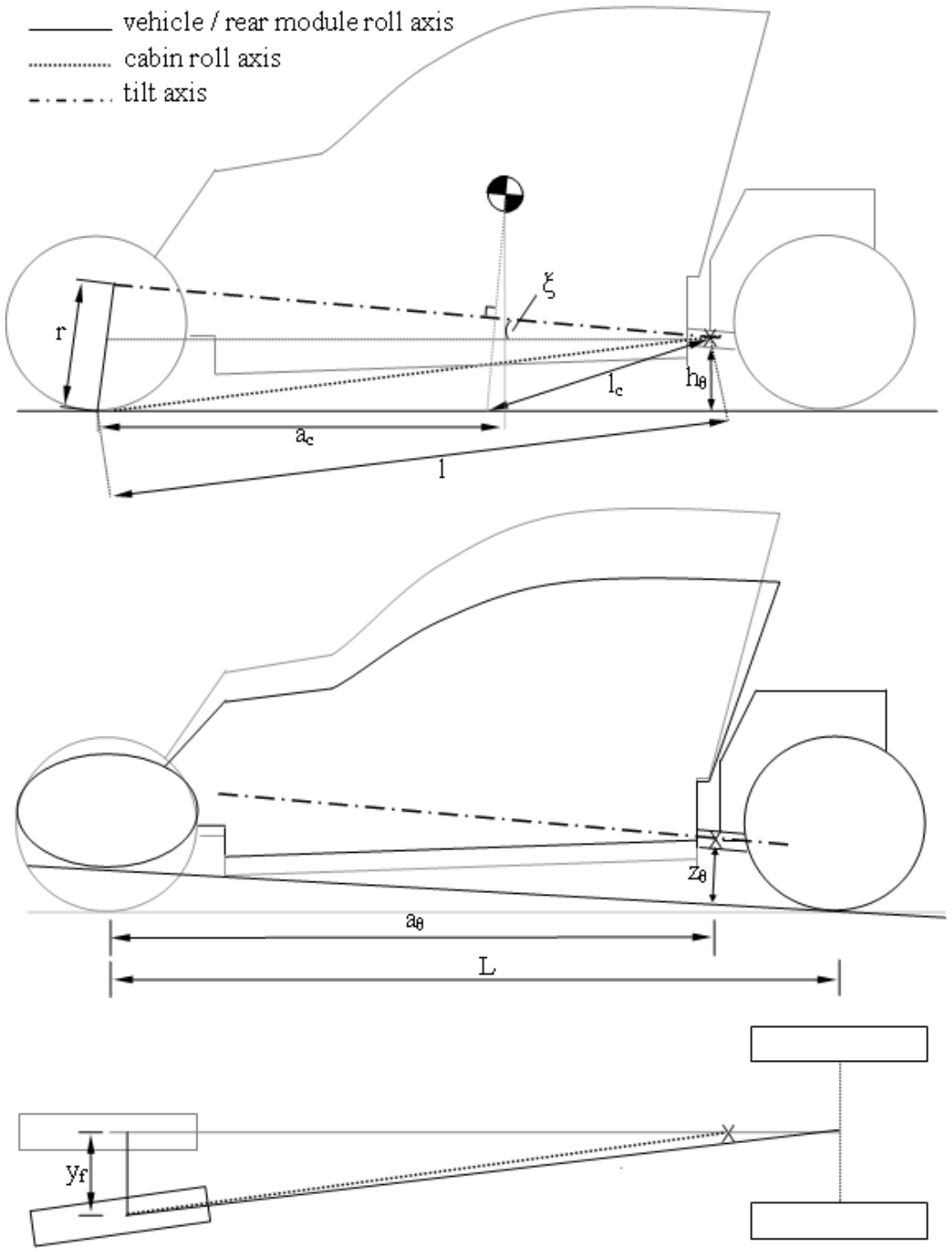

Figure 7: Vehicle roll axis before and after a rotation of the cabin about the tilt axis when keeping the rear module fixed

$$M_x L = [(m_f L - bm)z_{c\theta} + bmz_c]a_y - [bmy_{fc} + (m_f L - bm)y_c]g + LI_c\ddot{\theta} \tag{30}$$

The transfer functions relating the moment about the tilt bearing M_x to the tilt angle θ (G_3) and over the lateral acceleration a_y (G_4) are then given by:

$$G_3 = \frac{(LI_c)s^2 - (bmy_{fc} + (m_f L - bm)y_c)g}{L} \tag{31}$$

$$G_4 = \frac{((m_f L - bm)z_{c\theta} + bmz_c)}{L} \tag{32}$$

where

$$M_x = G_3\theta + G_4 a_y \tag{33}$$

3.3 Suspension Dynamics

At the principal frequencies (0-2Hz) of interest, the roll dynamics are dominated by the suspension and the tyre stiffnesses can be neglected. It has been shown that the roll dynamics can be uncoupled from the plane dynamics [14] and it is therefore possible to model the rear module as a single degree of freedom system. The roll of the rear module is then given by the following equation:

$$\begin{aligned}(I_r + I_c)\ddot{\phi} = &-\frac{T^2}{2}\phi K_s - \frac{T^2}{2}\dot{\phi}C_s - m_c g h_{r\theta}\phi + \frac{b}{L}mgh_{r\theta}\phi + m_c a_y h_{r\theta} - \frac{b}{L}mh_{r\theta}a_y \\ &- \frac{a}{L}mh_r a_y - K_{r\phi}\phi - M_x + \frac{1}{L}(bmy_{fc} + (m_c L - bm)y_c)g\phi\end{aligned} \tag{34}$$

The final term represents the additional moment about the tilt bearing cause by the extra cabin tilt angle associated with the suspension roll. The suspension stiffness and damping coefficients are give by K_s and C_s respectively. $K_{r\psi}$ is the roll-bar stiffness and $h_r\theta$ is the distance between the rear module CoG and the tilt bearing.

The above equation can be represented in state-space with the state vector x and input vector u:

$$x = \begin{bmatrix} \phi \\ \dot{\phi} \end{bmatrix} \qquad u = \begin{bmatrix} a_y \\ M_x \end{bmatrix} \tag{35}$$

The output variable y is the load transfer $\Delta F_z = -(\phi K_s + \dot{\phi} C_s)\frac{T}{2}$. The A, B, C and D matrices are then given by:

$$A = \begin{bmatrix} 0 & 1 \\ (-\frac{T}{2}K_s - m_c g h_{r\theta} + \frac{b}{L} m g h_{r\theta} - K_{r\phi} \\ +\frac{1}{L}(bmy_f c + (m_f L - bm)y_c)g)\frac{1}{(I_r + I_c)} & -\frac{T^2 C_s}{2(I_r + I_c)} \end{bmatrix}$$

$$B = \begin{bmatrix} 0 & 0 \\ (m_c h_{r\theta} - \frac{b}{L} m h_{r\theta} \\ -\frac{a}{L} m h_r a_y)\frac{1}{(I_r + I_c)} & -\frac{1}{(I_r + I_c)} \end{bmatrix}$$

$$C = -\begin{bmatrix} \frac{TK_s}{2} & \frac{TC_s}{2} \end{bmatrix}$$

$$D = \begin{bmatrix} 0 & 0 \end{bmatrix}$$

The transfer functions relating the load transfer to the input variables are obtained:

$$\Delta F_z = G_5 a_y + G_6 M_x \tag{36}$$

3.4 Valve and Actuator Dynamics

A schematic diagram of the hydraulic valve and actuator system is shown in figure 8.

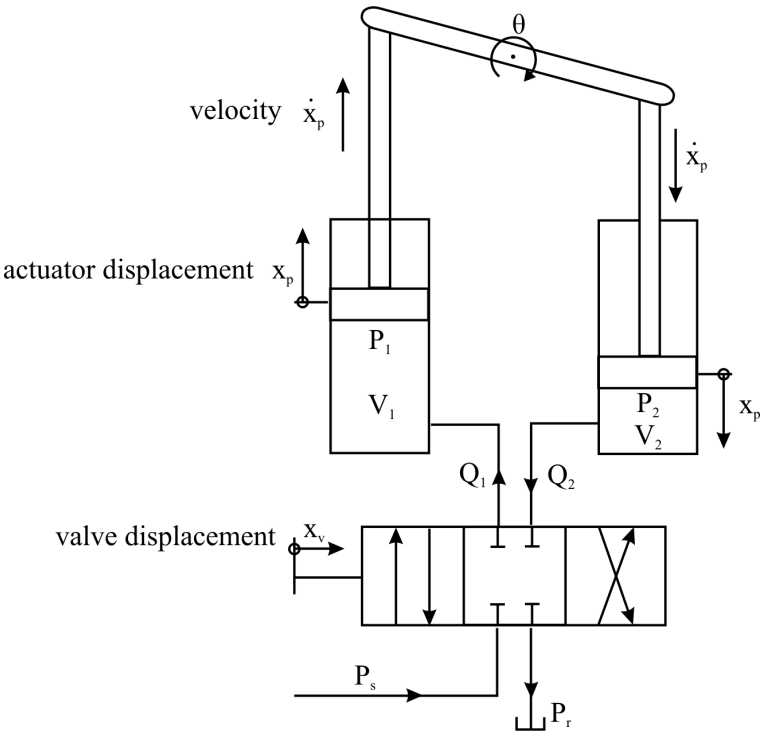

Figure 8: Representation of the valve and actuator system

Using small perturbation analysis, the linearised equation for the flow through the valve around the centre position is given by:

$$Q_L = K_q x_v + K_c \Delta P_L \tag{37}$$

where K_q and K_c are the flow gain and the pressure gain at the operating conditions, which are equivalent to the partial derivatives of the non-linear valve orifice equation:

$$Q = C_e x_{vo} \sqrt{P_s - \Delta P_{Lo}} \tag{38}$$

where ΔP_{Lo} is the load pressure on the system $(P_1 - P_2)$ and x_{vo} is the valve opening at the operating conditions. The values of K_q and K_c are therefore given by:

$$K_q = \frac{\partial Q}{\partial x_{vo}} = C_e\sqrt{P_s - \Delta P_{Lo}} \tag{39}$$

$$K_c = \frac{\partial Q}{\partial \Delta P_{Lo}} = \frac{-C_e x_{vo}}{\sqrt{P_s - \Delta P_{Lo}}} \tag{40}$$

The valve coefficient C_e is given by:

$$C_e = \frac{q_{nom}}{\sqrt{\frac{\Delta P_{nom}}{2}}} \tag{41}$$

A nominal flow q_{nom} of 16 l/min at a pressure drop ΔP_{nom} of 10 bar with 100% valve opening results in a valve coefficient value $C_e = 3.771 \cdot 10^{-7} m^4/s\sqrt{N}$. This value is calculated assuming that the valve opening is measured as a percentage of the maximum valve opening, i.e. when fully open $x_v = 1$.

The values of ΔP_{Lo} and x_{vo} were taken as averages from a non-linear simulation. This results in the values $5.504 \cdot 10^{-4}$ and $-3.187 \cdot 10^{-12}$ for K_q and K_c respectively.

The flows into the left and right actuators are given by:

$$Q_1 = A_p \dot{x}_p + q_{c1} \tag{42}$$

$$Q_2 = A_p \dot{x}_p - q_{c2} \tag{43}$$

where q_c is the flow into the volume due to the effect of increases in pressure. Therefore:

$$q_{c1} = \frac{V_1}{\beta}\frac{dp_1}{dt} = \frac{V_1}{\beta_e} s P_1 \tag{44}$$

$$q_{c2} = \frac{V_2}{\beta}\frac{dp_2}{dt} = \frac{V_2}{\beta_e} s P_2 \tag{45}$$

where s is the differential operator and V_1 and V_2 are the volumes in each hydraulic cylinder and depend on the position of the actuator piston:

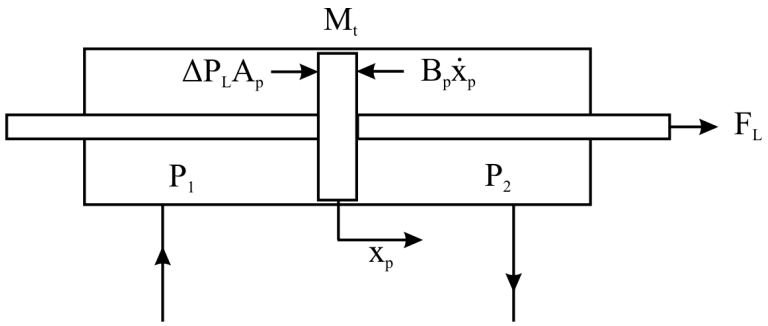

Figure 9: Forces acting upon a double ended actuator

$$V_1 = V_0 + A_p x_p \tag{46}$$

$$V_2 = V_0 - A_p x_p \tag{47}$$

V_0 represents the volume of fluid with the actuator in the central position. Rearranging equations 42 to 45, we get an expression for the pressures P_1 and P_2 at either side of the piston.

$$P_1 = (Q_1 - A\dot{y})\frac{\beta}{V_1}\frac{1}{s} \tag{48}$$

$$P_2 = (A\dot{y} - Q_2)\frac{\beta}{V_2}\frac{1}{s} \tag{49}$$

In the central position, V_1 and V_2 are equal to $\frac{V_t}{2}$ and Q_1 and Q_2 are equal to Q_L, ΔP_L $(P_1 - P_2)$ is therefore given by:

$$\Delta P_L = (Q_L - A_p x_p s)\frac{4\beta_e}{V_t s} \tag{50}$$

As the system is linearised about the central position, it is possible to simplify the actuator system by modelling the two actuators as a single double-ended actuator as shown in figure 9.

Resolving the forces acting on the piston:

$$M_t\ddot{x}_p = A_p\Delta P_L - B_p\dot{x}_p + F_L \tag{51}$$

This gives the transfer function:

$$x_p = \frac{A_p\Delta P_L + F_L}{M_t s^2 + B_p s} \tag{52}$$

The hydraulic system can be represented by the block diagram shown in figure 10.

Substituting for ΔP_L using equation 50:

$$x_p = G_9 x_v + G_{10} F_L \tag{53}$$

The transfer functions G_9 and G_{10} can be obtained by manipulating the block diagram:

$$G_9 = \frac{\frac{K_q}{A_p}}{\frac{V_t M_t}{4\beta_e A_p^2}s^3 + (\frac{V_t B_p}{4\beta_e A_p^2} - \frac{K_c M_t}{A_p^2})s^2 + (1 - \frac{B_p K_c}{A_p^2})s} \tag{54}$$

$$G_{10} = \frac{V_t s - 4\beta_e K_c}{(M_t V_t)s^3 + (B_p V_t - 4\beta_e K_c M_t)s^2 + (4\beta_e(A_p^2 - B_p K_c))s} \tag{55}$$

By neglecting the external load and including the tilt angle feedback loop, the closed loop hydraulic circuit can be represented by the block diagram shown in figure 11.

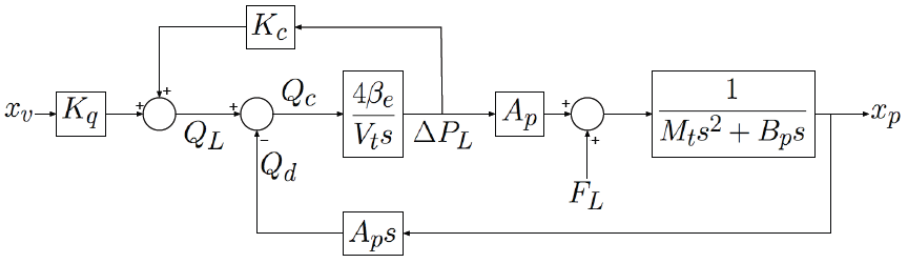

Figure 10: Linearised block diagram of hydraulic system [6]

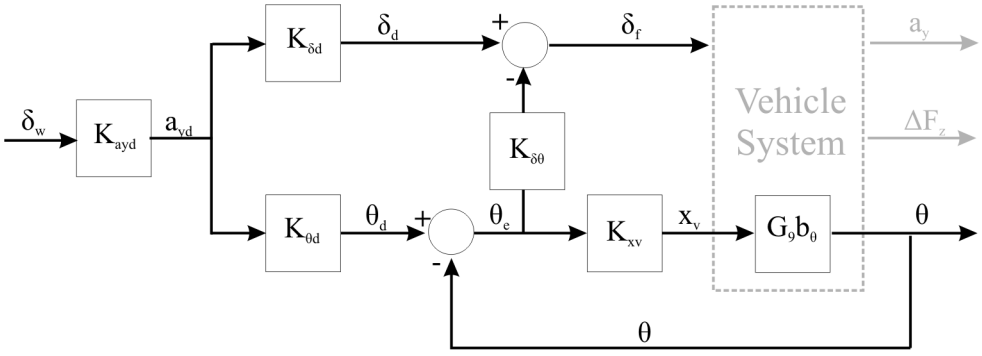

Figure 11: Controller including position feedback control of the hydraulic system

The transfer function relating θ to θ_d is then given by:

$$\begin{aligned}
\frac{\theta}{\theta_d} &= \frac{G_9 K_{xv} b_\theta}{1 + G_9 K_{xv} b_\theta} \\
&= \frac{\frac{K_q}{A_p} K_{xv} b_\theta}{\frac{V_t M_t}{4\beta_e A_p^2} s^3 + (\frac{V_t B_p}{4\beta_e A_p^2} - \frac{K_c M_t}{A_p^2}) s^2 + (1 - \frac{B_p K_c}{A_p^2}) s + \frac{K_q}{A_p} K_{xv} b_\theta} \\
&= \frac{\frac{K_q K_{xv} A_p b_\theta}{A_p^2 - B_p K_c}}{\left(\frac{s^2}{\omega_n^2} + \frac{2\zeta}{\omega_n} s + 1\right) s + \frac{K_q K_{xv} A_p b_\theta}{A_p^2 - B_p K_c}}
\end{aligned} \tag{56}$$

By neglecting the higher order dynamics that are significant at frequencies above the vehicle dynamics, the system can be simplified to a first order lag with a time constant τ, giving the transfer function G_{9a}:

$$G_{9a} = \frac{\theta}{\theta_d} = \frac{1}{1 + \tau s}$$

where

$$\tau = \frac{A_p^2 - B_p K_c}{K_q K_{xv} A_p b_\theta} \tag{57}$$

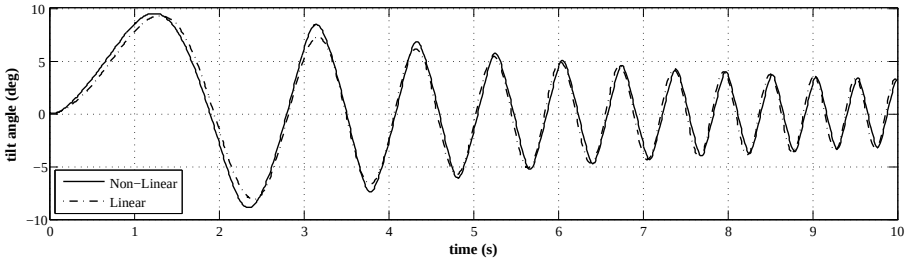

Figure 12: Non-linear tilt angle response and first order linear fit

This approximation assumes that the relationship between the tilt demand and achieved tilt angle is only dependent on the actuator dynamics. Although the assumption significantly simplifies the resulting transfer functions, it still offers a good match to the non-linear hydraulic performance resulting from a tilt angle demand input. Figure 12 shows the tilt angle response resulting from a 0.1 to 2Hz sweep in tilt angle demand as calculated by the non-linear model and the response obtained using the first order lag G_{9a}. As a good fit is obtained, the simplified hydraulic model will be used for the subsequent analysis.

3.5 Control System Transfer Function

Using the same techniques as in the previous section, the transfer function relating the actual steer angle δ_f to the demand steer angle δ_d is given by:

$$G_{11} = \frac{\delta_f}{\delta_d} = 1 - \frac{\tau s}{1+\tau s}\frac{K_{\theta d}K_{\delta\theta}}{K_{\delta d}} \tag{58}$$

Setting $K_{\delta\theta} = 0$ results in the original direct tilt control method.

3.6 Vehicle System Transfer Functions

With the simplifications previously described, the vehicle system can be described by the transfer function matrix:

$$\begin{bmatrix} a_y \\ \Delta F_z \end{bmatrix} = \begin{bmatrix} P_{11} & P_{12} \\ P_{21} & P_{22} \end{bmatrix} \begin{bmatrix} \delta_f \\ \theta_d \end{bmatrix} \tag{59}$$

where

$$P_{11} = \frac{a_y}{\delta_f} = G_1 \tag{60}$$

$$P_{12} = \frac{a_y}{\theta_d} = \frac{\theta}{\theta_d} \cdot \frac{a_y}{\theta} = G_{9a} G_2 \tag{61}$$

$$P_{21} = \frac{\Delta F_z}{\delta_f} = \frac{a_y}{\delta_f} \cdot \frac{\Delta F_z}{a_y} + \frac{a_y}{\delta_f} \cdot \frac{M_x}{a_y} \cdot \frac{\Delta F_z}{M_x} = G_1 G_5 + G_1 G_4 G_6 \tag{62}$$

$$\begin{aligned} P_{22} = \frac{\Delta F_z}{\theta_d} &= \frac{\theta}{\theta_d} \cdot \frac{a_y}{\theta} \cdot \frac{M_x}{a_y} \cdot \frac{\Delta F_z}{M_x} + \frac{\theta}{\theta_d} \cdot \frac{M_x}{\theta} \cdot \frac{\Delta F_z}{M_x} + \frac{\theta}{\theta_d} \cdot \frac{a_y}{\theta} \cdot \frac{\Delta F_z}{a_y} \\ &= G_{9a} G_2 G_4 G_6 + G_{9a} G_3 G_6 + G_{9a} G_2 G_5 \end{aligned} \tag{63}$$

Finally, to obtain δ_f and θ_d as a function of the lateral acceleration demand a_{yd}:

$$\begin{bmatrix} \delta_d \\ \theta_d \end{bmatrix} = a_{yd} \begin{bmatrix} K_{\delta d} G_{10} \\ K_{\theta d} \end{bmatrix} \tag{64}$$

The vehicle system parameter values are listed in table 1.

4 Non-Linear Multi-Body Model

A full multi-body model of the vehicle was developed in SimMechanics [14], in order to account for non-linear effects and to compare with the linear model. Using a 3 dimensional multi-body modelling approach also includes coupling effects of various modes. Furthermore, the vehicle kinematics can be accurately represented. The model was

Table 1: Vehicle system parameters

Lateral Dynamics		
Dist. CoG to front	a	1.56 m
Dist. CoG to rear	b	0.84 m
Front tyre slip stiffness	$C_{\alpha f}$	13.6 kNrad^{-1}
Rear tyre slip stiffness	$C_{\alpha r}$	15.7 kNrad^{-1}
Front tyre camber stiffness	$C_{\theta f}$	1.2 kNrad^{-1}
Cabin yaw inertia	I_z	235.5 kgm^2
Rear steer coefficient	$K_{\delta r}$	0.181
Vehicle wheelbase	L	2.4 m
Total system mass	m	408 kg
Forward velocity	V	30 kmh^{-1}
Kinematics and Cabin Moment		
See figure 7	a_c	1.14 m
See figure 7	a_θ	1.95 m
Height of cabin CoG	h_c	0.59 m
Height of rear module CoG	h_r	0.54 m
Height of tilt joint	h_θ	0.271 m
See figure 7	l	1.97 m
See figure 7	l_c	0.904 m
Cabin mass	m_c	250 kg
Rear module mass	m_r	162 kg
Rear module track	T	0.84 m
Tilt axis angle	ξ	5°
Suspension Dynamics		
Rear suspension damping	C_s	1890 Nsm^{-1}
Roll inertia of cabin	I_c	100 kgm^2
Roll inertia of rear module	I_r	13.3 kgm^2
Rear suspension spring stiffness	K_s	21 kNm^{-1}
Valve and Actuator Dynamics		
Actuator piston area	A_p	$8.043 \cdot 10^{-4}$m^2
Actuator tilt/displacement ratio	b_θ	7.27 rad^{-1}
Viscous damping of actuator	B_p	2000 Nsm^{-1}
Valve coefficient	C_e	$3.771 \cdot 10^{-7}$
Flow gain	K_q	$5.505 \cdot 10^{-4}$
Pressure gain	K_c	$-3.187 \cdot 10^{-12}$
Actuator piston mass	M_t	2 kg
Supply pressure	P_s	160 bar
Hydraulic system volume	V_t	$2.011 \cdot 10^{-4}$ m^3
Effective bulk modulus	β_e	4500 bar

validated using data from numerous experimental tests performed with the prototype vehicle [14].

Figure 13 is an image generated in the SimMechanics model visualisation mode. The image is presented as an overlay on top of an image of CLEVER such that the individual bodies can be associated with each part of the vehicle. The individual bodies and their properties are listed in table 2. The values of mass and inertia were obtained through measurements as well as using CAD model data. The actuators and suspension struts were also modelled as two mass systems. Their mass and inertia values have not been listed as they are small compared to the other main bodies.

The hydraulic system was modelled using the non-linearised equations 38 and 41 to 49 discussed previously, where the actuators are individually actuated using the calculated hydraulic force. The suspension is modelled using separate compression and rebound damping coefficients. The slip angles are calculated using the non-linear equations 9 and 10 and the tyre models are presented in the following section.

4.1 Non-Linear Tyre Models

The non-linear force description of the front motorcycle tyre makes use of a simplified version of the magic formula [18]. As only the lateral motion of the vehicle is considered, the effects of fore and aft load transfer resulting from braking, accelerating and air drag have been omitted.

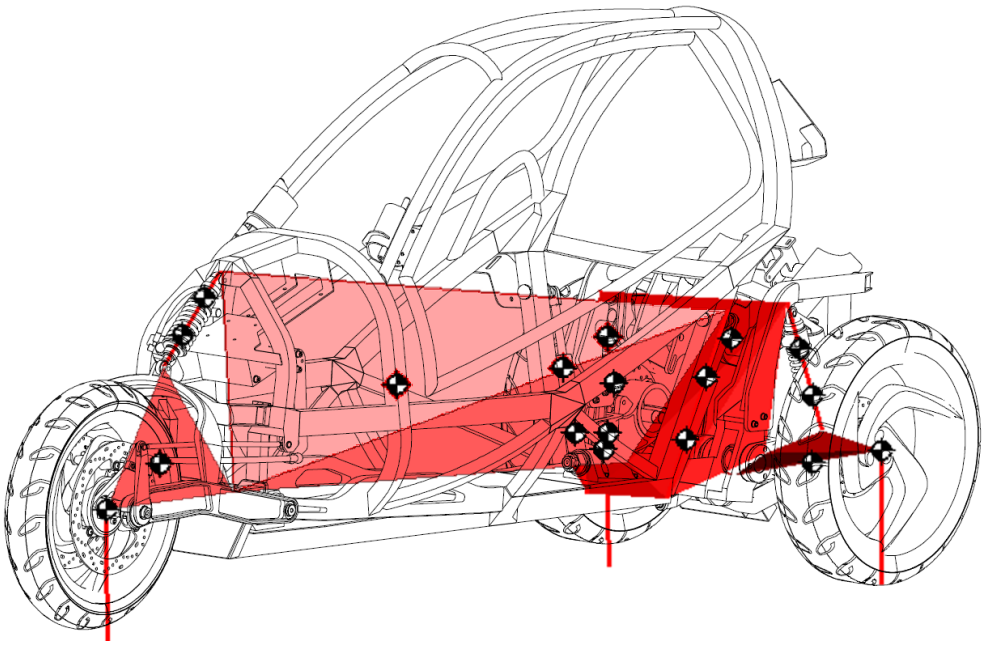

Figure 13: Vehicle multi-body model visualisation

Body	**Mass** $[kg]$	**Inertia** $[I_{xx} \quad I_{yy} \quad I_{zz}]$ $[kgm^2]$
Cabin	137	[14.5 200 170]
Rear Module	118	[13.3 13.3 13.3]
Driver	83	[8.2 7.3 1.4]
Front Swingarm	18	[0.43 0.60 0.77]
Rear Swingarms	15	[0.048 0.1 0.37]
Front Wheel	12	[0.27 0.54 0.27]
Rear Wheel	12	[0.27 0.54 0.27]

Table 2: Weight and inertia of main model components

$$F_y = D\sin[C\tan^{-1}(B(\alpha' + S_H))] + S_V \quad (65)$$

$$C = d_8 \quad (66)$$

$$D = \frac{d_4 F_z}{1 + d_7\gamma^2} \quad (67)$$

$$B = \frac{C_\alpha}{CD} \quad (68)$$

$$S_{Hf} = \frac{C_\gamma \gamma'}{C_\alpha} \quad (69)$$

$$S_V = d_6 F_z \gamma' \quad (70)$$

$$S_H = S_{Hf} - \frac{S_V}{C_\alpha} \quad (71)$$

The values for the parameters involved have been listed in table 3. The parameters $d_4 - d_8$ relating to the non-linear region of the slip - lateral force curve were taken from Pacejka's tyre model [18].

The rear tyres were modelled based on Pacejka's 'Magic Formula' or semi-empirical tyre model for car tyres. Due to the limiting testing facilities available, the Similarity Method [18] was used to determine the parameters. This method is based on the observation that the pure slip curves remain approximately similar in shape when the tyre runs at conditions that are different from the reference condition. For the purposes of this study, the reference condition is defined as the state where the tyre runs at its nominal load (F_{z0}) at camber angle equal to zero ($\gamma = 0$), free rolling and on a given road surface (μ_0). A similar shape means that the characteristics that belong to the reference condition is regained by shifting and multiplication in the horizontal and vertical direction. A demonstration that in practice similarity does indeed occur is given by Radt and Milliken [19] and by Milliken and Milliken [20]. The formula used to calculate the lateral force is shown in equation 72.

C_α	9.74 F_z	d_4	1.2	d_7	0.15
C_γ	0.86 F_z	d_6	0.1	d_8	1.6

Table 3: Front Tyre Magic Formula Parameters

$$y = D\sin[C\tan^{-1}(Bx - E(Bx - \tan^{-1}Bx))] \tag{72}$$

with

$$F_y = y(x) + S_v \tag{73}$$

$$x = \tan\alpha + S_h \tag{74}$$

and the other variables are as follows:

- B: stiffness factor
- C: shape factor
- D: peak value
- E: curvature factor
- S_h: horizontal shift
- S_v: vertical shift

The cornering stiffness is given as a function of the wheel load:

$$C_\alpha = c_1 c_2 F_{zo} \sin\left(2\tan^{-1}\left(\frac{F_z}{F_z o}\right)\right) \tag{75}$$

The peak factor for the side force is given by:

$$D_o = \mu_0 F_{zo} \tag{76}$$

The stiffness factor is given by:

$$B_o = \frac{C_\alpha}{CD_o} \tag{77}$$

Finally, the side force at nominal load F_{zo} is given by:

$$F_{yo} = D_o \sin[C \tan^{-1}(B_o x - E(B_o x - \tan^{-1} B_o x))] \tag{78}$$

where $x = \tan \alpha$.

The wheel load affects both the peak level (where the saturation of the curve takes place) and the slope where $\alpha \to 0$ i.e. the slip stiffness C_α. The first effect is obtained by multiplying the original characteristic equation by the ratio F_z/F_{zo}. This results in the new function:

$$F_y = \frac{F_z}{F_{zo}} F_{yo}(\alpha_{eq}) \tag{79}$$

The second step in the manipulation of the original curve is the adaptation of the slope at $\alpha = 0$ which is achieved by horizontal multiplication of the new characteristic curve accomplished with the equivalent slip angle:

$$\alpha_{eq} = \frac{F_z o}{F_z} \alpha \tag{80}$$

As the rear module rolls, small levels of camber thrust will be introduced as a result of the rear wheel camber $\gamma_r = \phi$. For small angles the camber thrust generated by the rear tyres can be approximated by the product of the camber stiffness and the camber angle [18]. This results in a horizontal shift S_h of the α_r against F_{yr} curve equivalent to:

$$S_h = \frac{C_\gamma(F_z)}{C_\alpha(F_z)} \gamma \tag{81}$$

This gives the equivalent slip angle α_{eq} (equation 80) where α is replaced with $\alpha + S_h$.

F_{zo}	3000N	C	1.3	c_1	8	μ_0	1
F_z	1350N	E	-1	c_2	1.33		

Table 4: Rear tyre magic formula parameters

5 Linear Model Results

Using the linear model transfer functions, a good correlation was obtained between the linear and non-linear model. Although a good fit was found up to frequencies of 10Hz, the results are displayed for 0.1 - 2Hz as this largely encompasses the frequencies that can be encountered when the vehicle is driven.

Figures 14 and 15 show the linear and non-linear lateral acceleration and rear axle load transfer response for a chirp steer input at the steering wheel of $\pm$ 45°with driving speed of 30km/h. This is equivalent to a steering angle at the wheel δ_f of $\pm$ 3.8°. It can be seen that the linear and non-linear results remain very close across the entire frequency range. Figures 16 and 17 show the lateral acceleration and load transfer response for a chirp tilt demand input θ_d of $\pm$ 10° at 30km/h. Figure 16 shows a good match for the lateral acceleration response across the entire frequency range. The load transfer shown in figure 17 exhibits more error at lower frequencies, where the non-linear model appears to have a phase lag when compared to the linear model. It can be seen that the load transfer response is more non-linear at the lower frequencies than at higher frequencies. This is likely to be because the gravitational forces acting on the cabin are more significant at lower frequencies.

The combined lateral acceleration and load transfer response is shown in figures 18 and 19. This represents the vehicle response under normal operating conditions, i.e. the steering angle input from the driver is used in conjunction with the vehicle speed to calculate the tilt angle demand (equation 4). There is still a reasonable match between the linear and non-linear results.

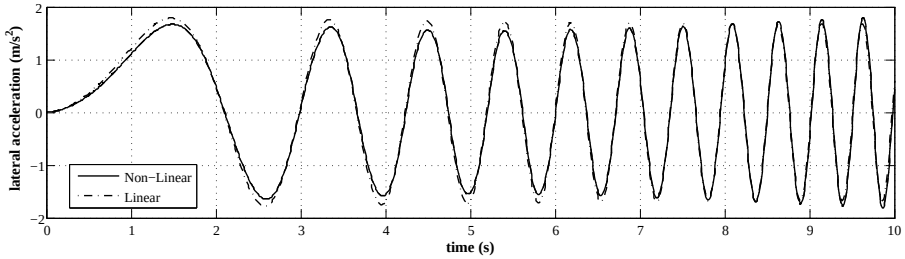

Figure 14: Linear and non-linear lateral acceleration response to a steer input

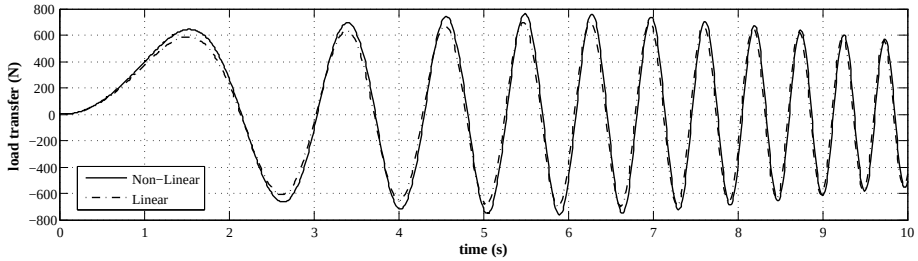

Figure 15: Linear and non-linear load transfer response to a steer input

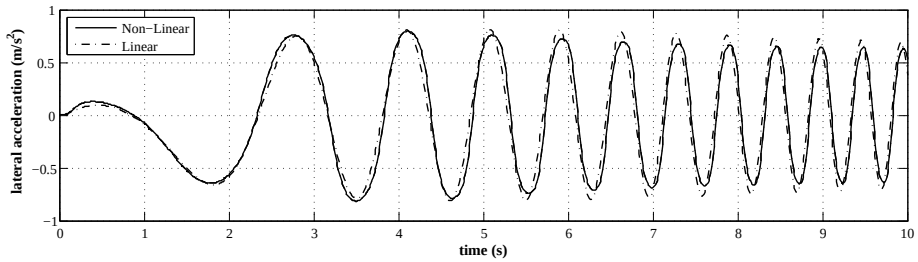

Figure 16: Linear and non-linear lateral acceleration response to a tilt demand input

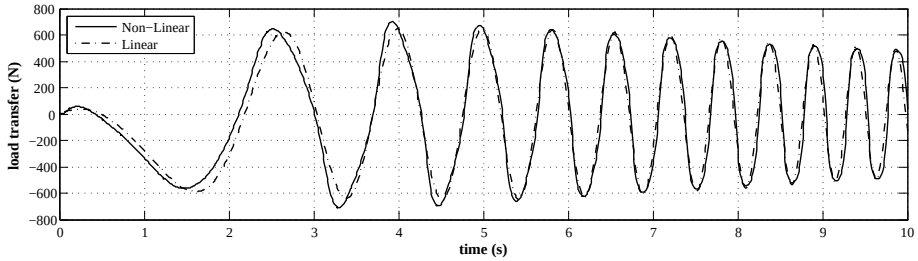

Figure 17: Linear and non-linear load transfer response to a tilt demand input

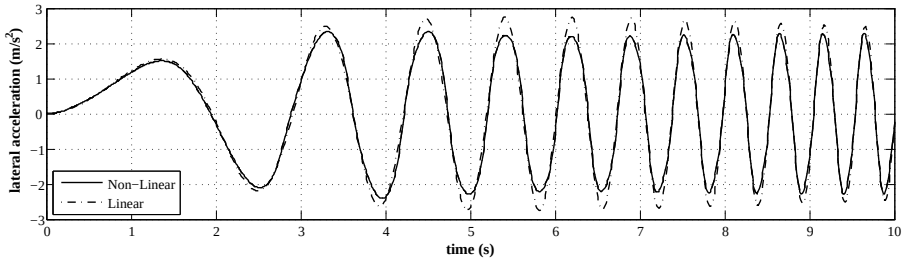

Figure 18: Linear and non-linear lateral acceleration response to a combined steer and tilt demand input

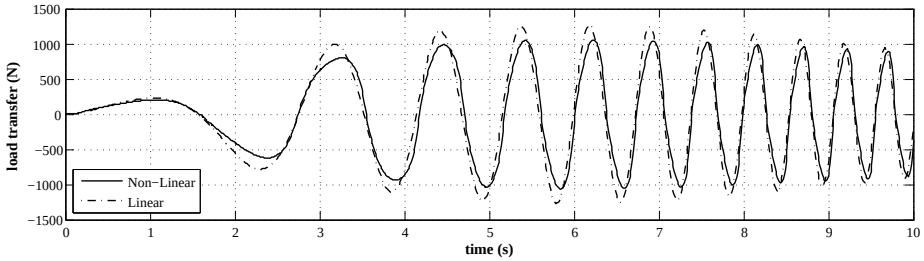

Figure 19: Linear and non-linear load transfer response to a combined steer and tilt demand input

6 Frequency Domain Analysis

Using the transfer functions from section 3.5, it is possible to plot the frequency response of the vehicle lateral acceleration and load transfer against the demand lateral acceleration, as shown in figures 20 and 21. It is worth noting that the lateral acceleration and load transfer response both reach a maximum amplitude between 1Hz and 2Hz and it was at this frequency that roll over problems were experienced with the prototype DTC vehicle.

With the confidence that the linear model gives a good representation of the system dynamics, it is possible to compare the original system response with that of the proposed controller over the entire frequency range of interest. Figures 22 and 23 show the lateral acceleration and load transfer response of the original DTC controller ($K_{\delta\theta} = 0$) compared to that of the proposed SDTC controller. The system response is shown for a range of steering gains $K_{\delta\theta}$ from 0.2 to 0.4. This range was chosen so that the lateral acceleration amplitude would never exceed the demand lateral acceleration am-

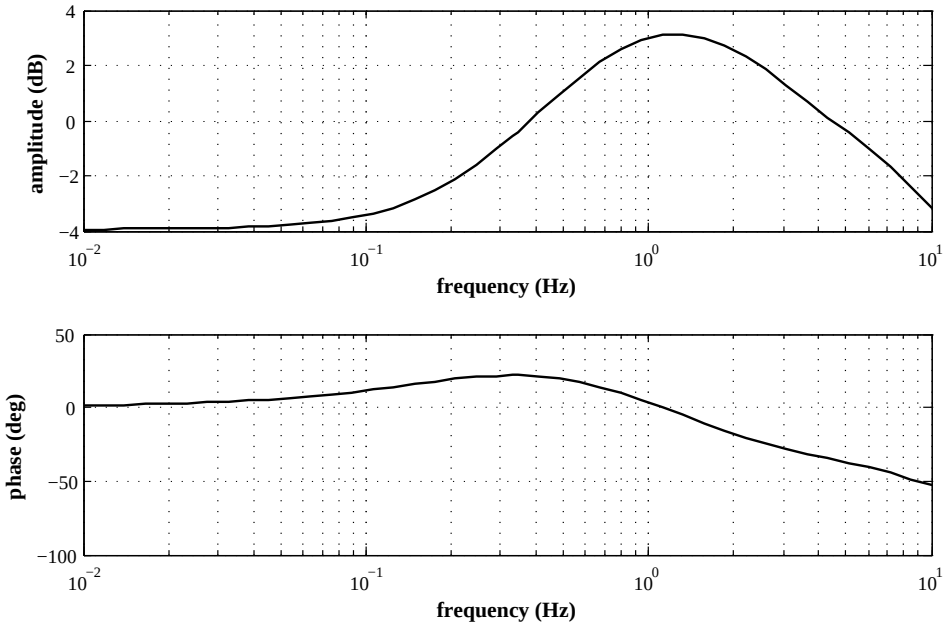

Figure 20: Bode plot of lateral acceleration response for original controller

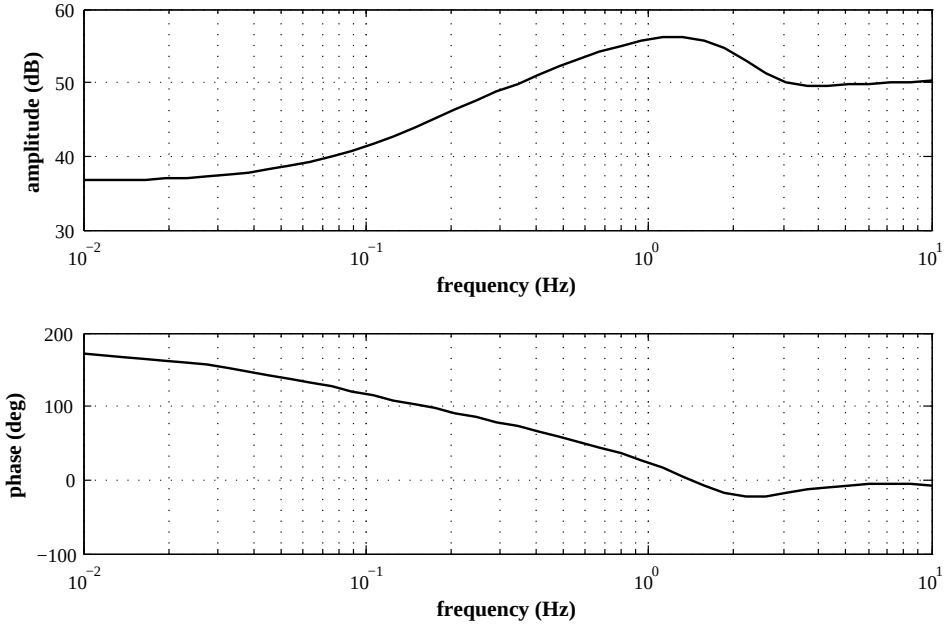

Figure 21: Bode plot of load transfer response for original controller

plitude. For the previous control method, the actual lateral acceleration can be seen to exceed the demand lateral acceleration over a significant part of the frequency range, leading to an increase in the load transfer. This would have been an important factor contributing to the tendency of the vehicle to roll. With the new control approach however, the lateral acceleration does not exceed the demand lateral acceleration. As a result, the load transfer is also reduced over the principal frequency range of 0.1 - 2Hz. It should be noted that at lower frequencies, the achieved lateral acceleration does not match the demand lateral acceleration due to the under-steer effect introduced by the kinematic rear-wheel steer [14]. With the correct amount of rear wheel steer, this would be much closer to 1 (0dB). In this case a higher steering gain $K_{\delta\theta}$ would be required to keep the ratio $\frac{a_y}{a_{yd}}$ as close as possible to 0dB over the principal frequency range. It can be argued that for a neutral and predictable handling response, the lateral acceleration response should remain constant across the frequency range. This can be achieved with a steering gain value of 0.4. By increasing the gain any further, the lateral acceleration response deviates further from the demand acceleration. Increasing the gain up to 0.4 also leads to a positive effect on the load transfer as can be seen in figure 23. The system response will be investigated in the time domain to confirm these findings.

7 Time Domain Response

The controller was tuned in the frequency domain with the system linearised about the centre position and a vehicle forward speed of 30 km/h. Performance will be investigated in the time domain with the non-linear model. As the principal aim of the controller is to improve transient performance, a number of manoeuvres will be investigated where the original control method would have brought the vehicle to the brink of roll-over (i.e. zero inner wheel load) and the vehicle dynamics of the original and new control approach are compared. A figure of eight manoeuvre requiring approximately 1.2kJ of energy from the actuators has been undertaken with the new control approach using the full non-linear simulation and the lateral acceleration and load transfer response is compared with the original response in figures 24 and 25.

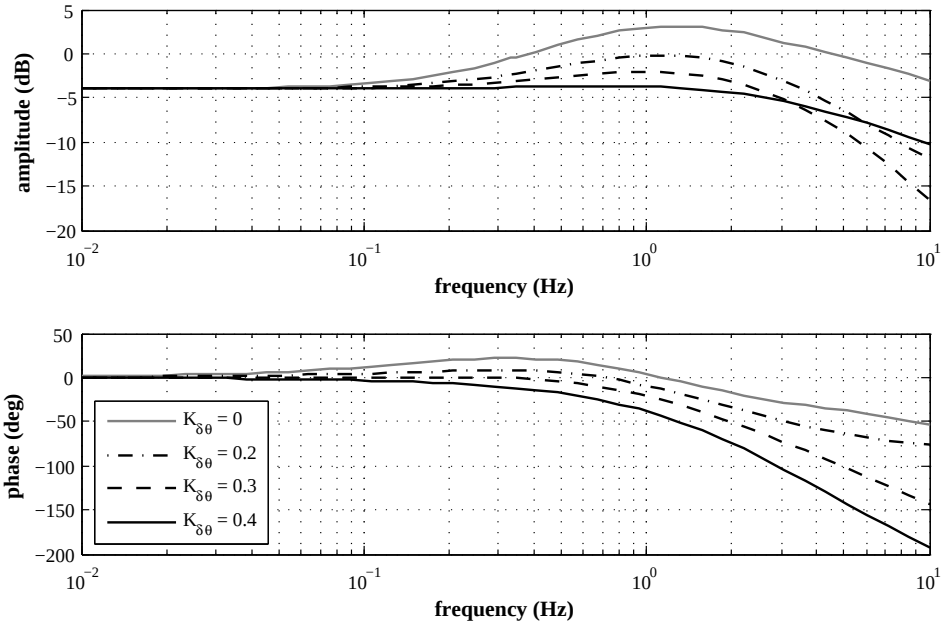

Figure 22: Bode diagram of $\frac{a_y}{a_{yd}}$ for original DTC ($K_{\delta\theta} = 0$) and new SDTC controller

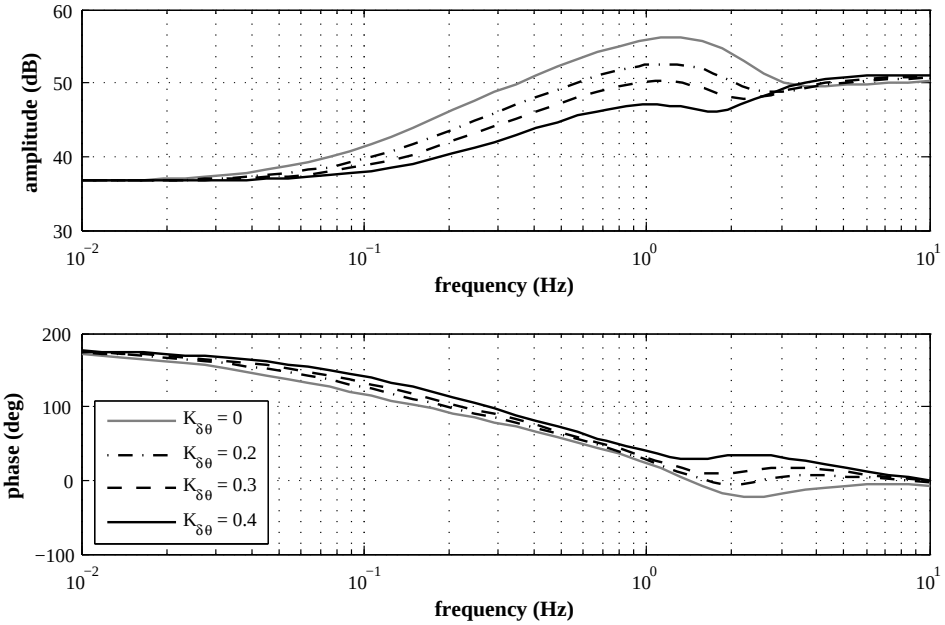

Figure 23: Bode diagram of $\frac{\Delta F_z}{a_{yd}}$ for original DTC ($K_{\delta\theta} = 0$) and new SDTC controller

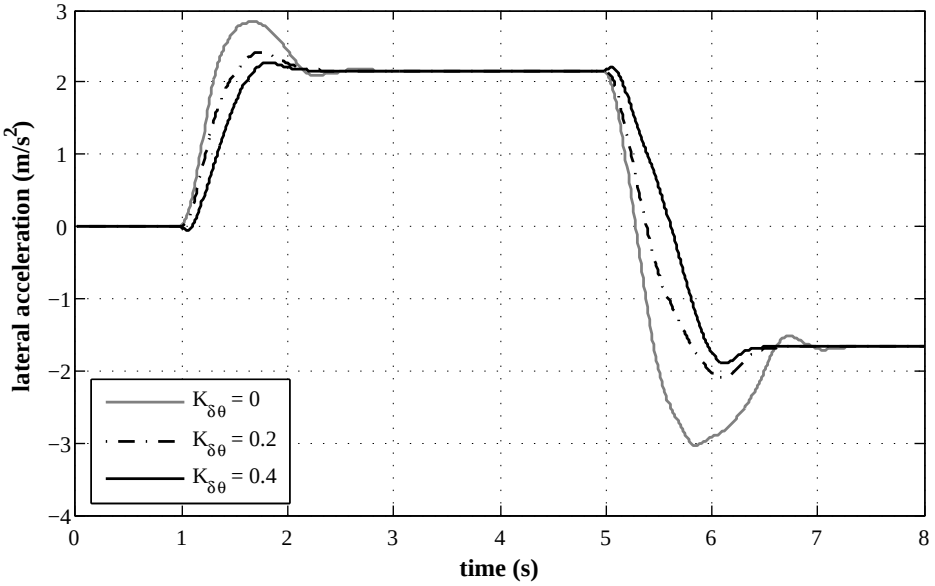

Figure 24: Lateral acceleration response for entering and exiting a steady state corner using the original DTC ($K_{\delta\theta} = 0$) and new SDTC controller

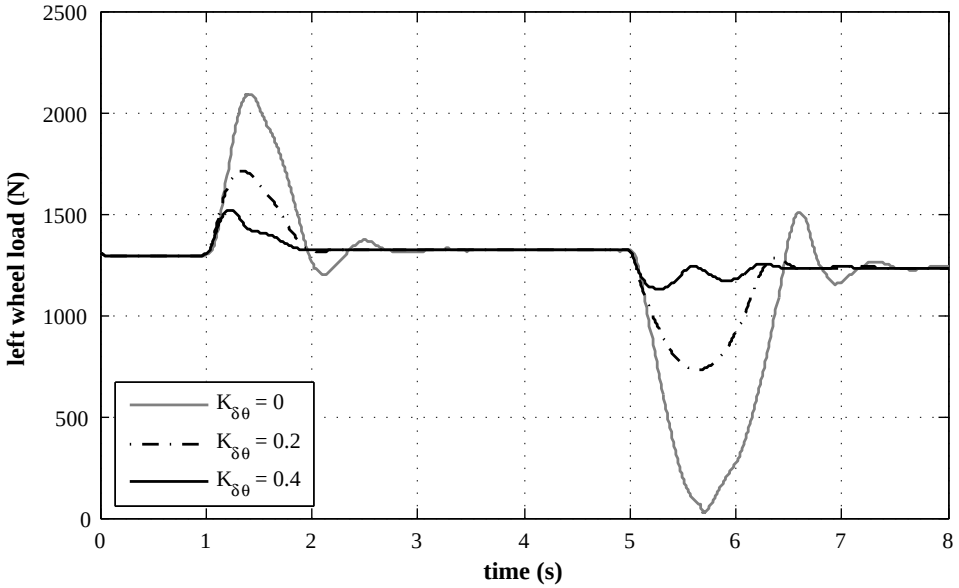

Figure 25: Left wheel load for entering and exiting a steady state corner using the original DTC ($K_{\delta\theta} = 0$) and new SDTC controller

Looking at figure 24, it can be seen that the lateral acceleration builds up more gradually with the new SDTC control approach. As a result, there is significantly less over-shoot and the lateral acceleration settles to the steady state value more rapidly. The more gradual build-up of lateral acceleration and reduced actuator loads lead to a significant reduction in the load transfer, as shown in figure 25. Whereas with the previous controller, this manoeuvre would almost lead to the vehicle rolling over, with the new strategy, the inner wheel load is still in a safe range.

The robustness of the new control method and the effect of the gain $K_{\delta\theta}$ can be investigated further by looking at the response to a step input requiring approximately 1.3kJ of energy from the actuators, which may have lead to the vehicle rolling over with the original control method. Looking at figure 26, it can be seen that increasing the gain results in some counter-steering. This results in an even smaller load transfer as can be seen in figure 28 and a faster response in the tilt angle as seen in figure 29. Furthermore, it has the positive effect of reducing over-shoot in the lateral acceleration and the lateral acceleration settles into steady state more rapidly. It could be argued that introducing some counter-steer would cause the vehicle to briefly travel in the opposite direction to that desired. However, with this control strategy, counter-steer would only occur in extreme situations, where it would be necessary to prevent roll-over. Furthermore, this would only occur for a fraction of a second, and would be unlikely to be noticed by the driver, similar to the counter-steering effects on a motorcycle. Looking at the lateral acceleration profile in figure 27, it can be seen that the proportion of time spent at a negative lateral acceleration is extremely small, but that the benefits in terms of load transfer are significant. A good value for the steering gain $K_{\delta\theta}$ at a driving speed of 30 km/h is confirmed to be 0.4.

The extended stability of the new controller with a steering gain $K_{\delta\theta}$ of 0.4 can be shown by a severe manoeuvre requiring 2.3kJ of energy that brings the vehicle to the brink of roll-over. This is shown in figures 30 and 31. At lateral accelerations of around 8m/s^2 the vehicle reaches the adhesion limit of the tyres where the dynamics become highly non-linear. At this point the inner wheel load almost reaches zero. However, it can be seen that there is very little additional load transfer as the vehicle tilts back

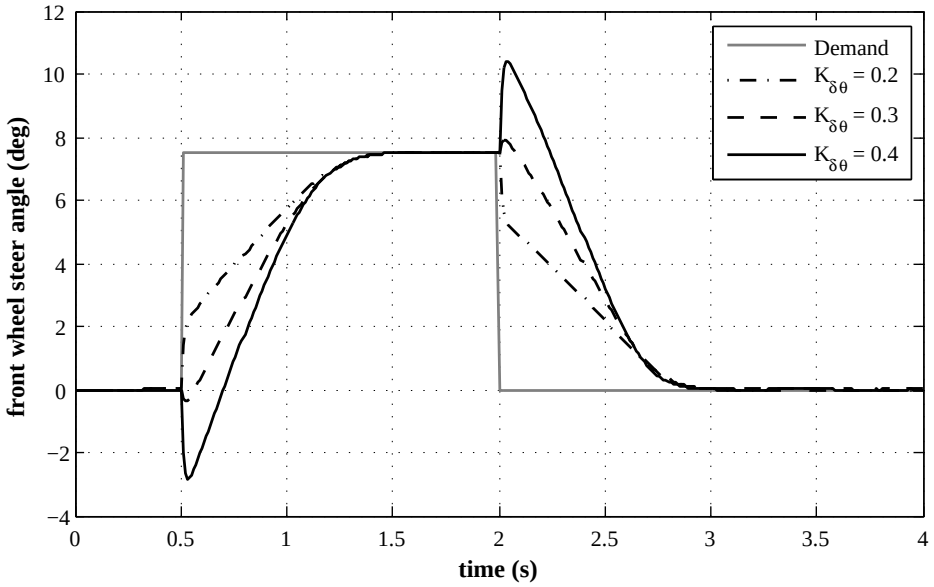

Figure 26: Steer response to a step input in the lateral acceleration demand

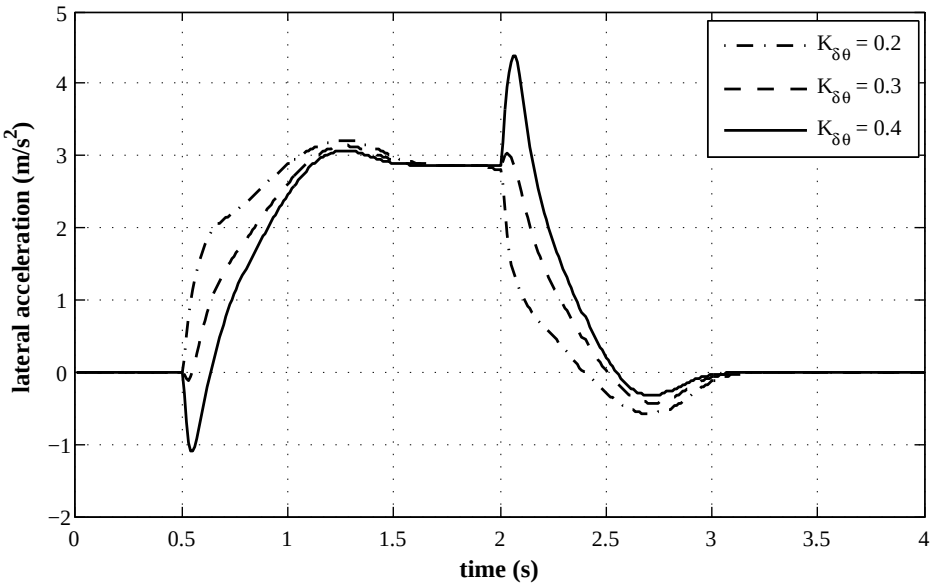

Figure 27: Lateral acceleration response to a step input in the lateral acceleration demand

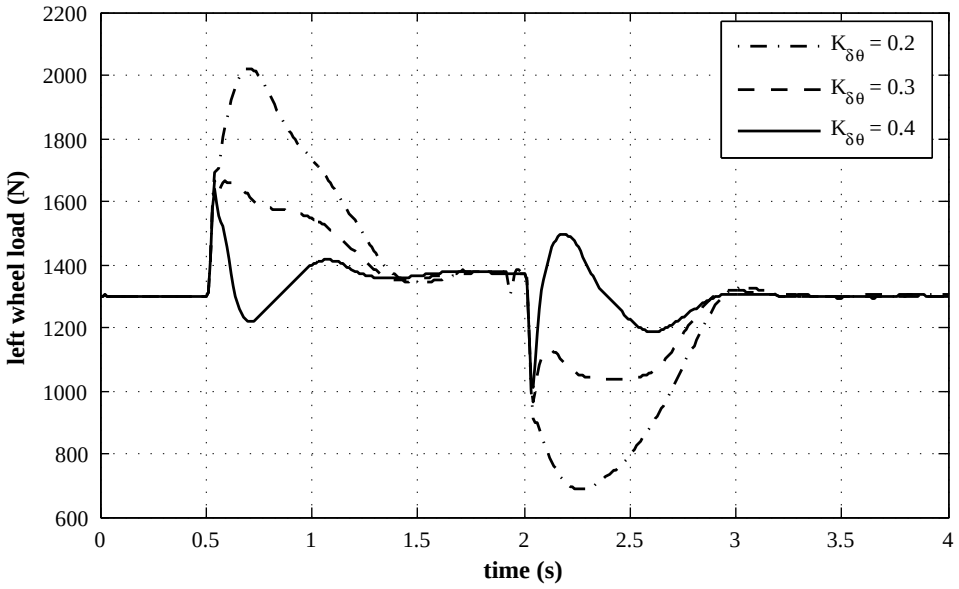

Figure 28: Left wheel load response to a step input in the lateral acceleration demand

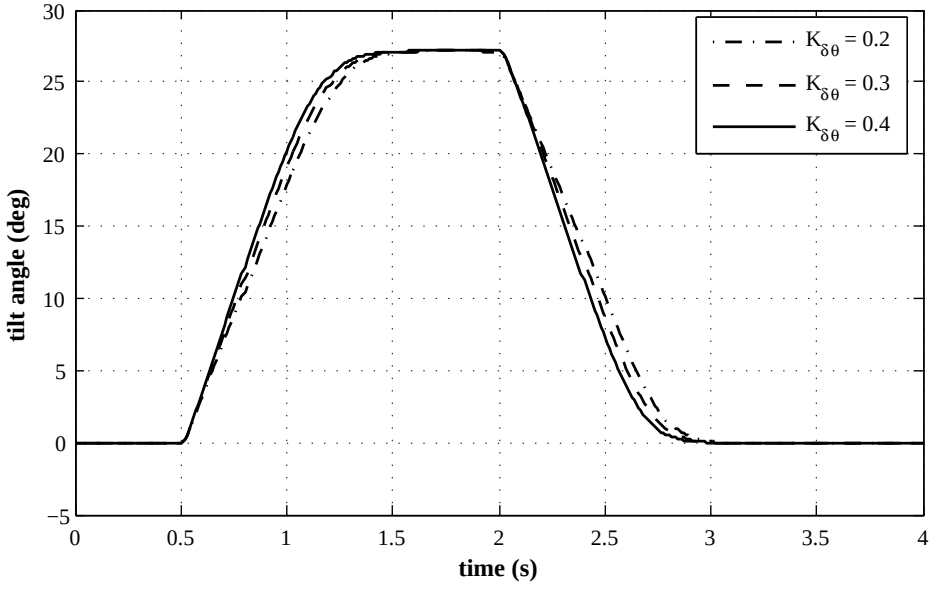

Figure 29: Tilt angle response to a step input in the lateral acceleration demand

to the original position. The new controller therefore allows the vehicle to be driven much closer to its physical limits.

The optimal steering gain is velocity dependent. The process was therefore repeated at 10km/h intervals up to 120km/h, which represents the operating range of the vehicle. The results are shown in figure 32. The optimal value was chosen as the minimum value of $K_{\delta\theta}$ that resulted in no increase in the $\frac{a_y}{a_{yd}}$ amplitude profile, similar to that obtained for $K_{\delta\theta} = 0.4$ at 30km/h. With the correct kinematic set-up, this should result in the lateral acceleration matching the lateral acceleration demand across the principal frequency range and give a safe and predictable handling performance.

It can be seen that the steering gain reaches horizontal asymptotes at each end of the speed range. At low speed there is very little lateral force resulting from a steer input and therefore steering gain has little effect. At high speed, the resultant forces are much larger and hence a smaller gain is required to achieve the desired response. The results shown in figure 32 could be applied as a look-up table in the vehicle controller.

8 Concluding Remarks

This paper presents a tilt control concept for a narrow track vehicle, and includes controller analysis and simulation results using both non-linear and linearised models. The linear model was shown to give a good fit to the non-linear model. The frequency domain response of an earlier DTC control system displayed a peak in the lateral acceleration and load transfer response between 1Hz and 2Hz, which matched the observations made previously in subjective tests. Around this frequency, the lateral acceleration was considerably higher than the demand lateral acceleration, as the initial steering input would lead to large slip angles at the front and rear. This leads to a large load transfer across the rear axle and is a significant factor contributing to the potential roll-over of the vehicle.

The proposed control system treats the driver steering input as a lateral acceleration

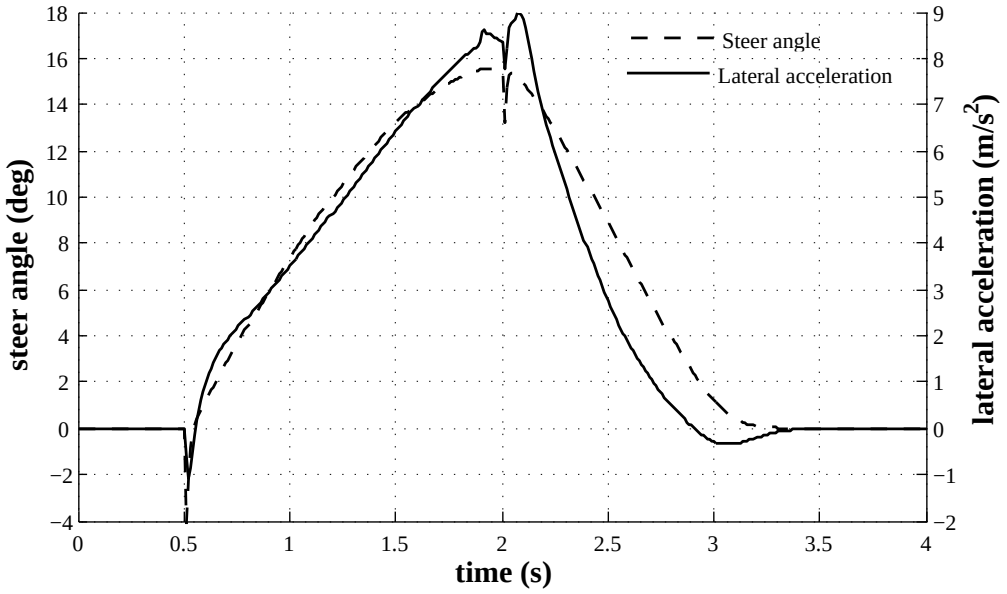

Figure 30: Steer and lateral acceleration response for a severe manoevre

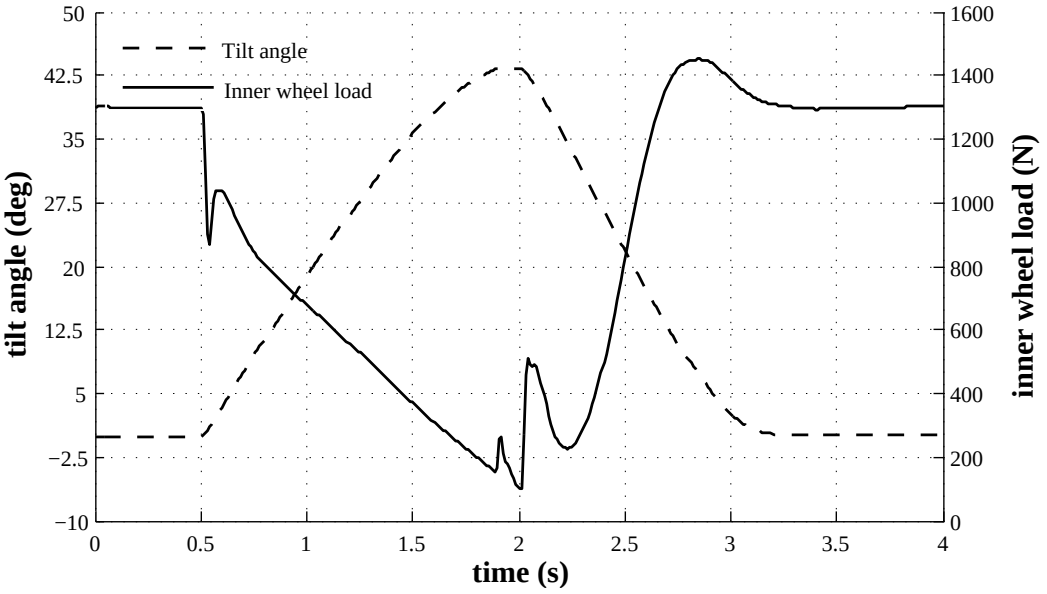

Figure 31: Tilt angle and inner wheel load response for a severe manoevre

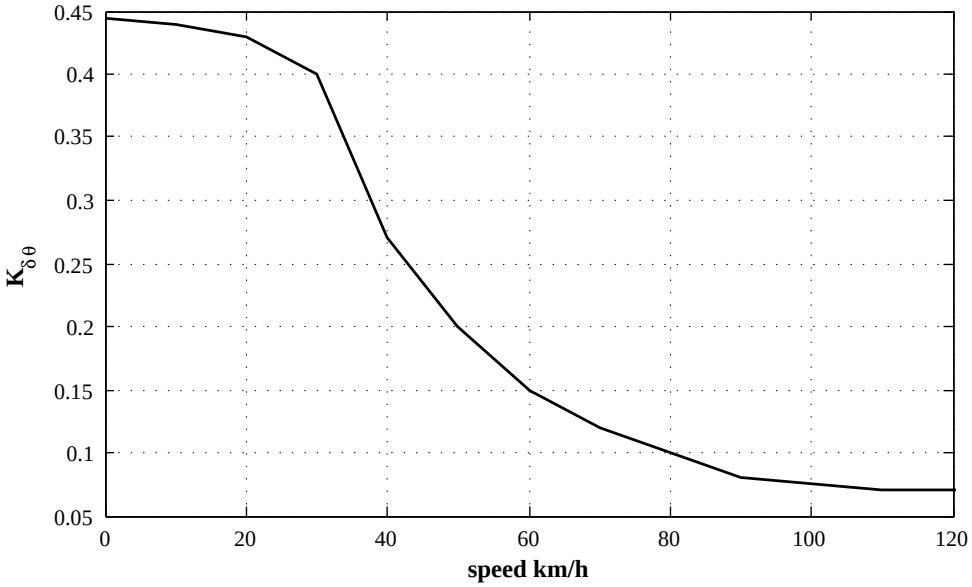

Figure 32: Steering gain against forward speed

demand that is to be reached as rapidly as possible and with minimum load transfer across the rear axle. It utilises a negative gain feedback between the tilt-error and the steer input, reducing the steering angle as the tilt error increases. As a result the forces which act on the actuator are significantly reduced and the desired tilt angle can be reached more rapidly and with less load transfer. The system model was linearised about the central position at a driving speed of 30km/h, and an ideal steering gain was determined from the model at this speed. The process was repeated in 10km/h intervals from 0 - 120km/h to obtain the steering gain over the speed range of the vehicle.

The frequency response analysis of the proposed SDTC control system indicated a much more predictable handling response than the original DTC controller, coupled with reduced load transfer across the rear axle. Using the non-linear model, the lateral acceleration response has less overshoot and the lateral acceleration settles to the steady state value more rapidly. The resultant rear axle load transfer for a demanding manoeuvre using the new control method was shown to be approximately 15% of the original value. The new control method was also shown to result in some counter-

steering in rapid steering manoeuvres. This helps to tilt the cabin to the desired tilt angle and simultaneously reduce load transfer. As a result the controller is shown to be very robust, even in extreme manoeuvres. Currently work is underway to implement the controller on the CLEVER vehicle.

List of Figures

Nomenclature

A_p	actuator piston area
a	londitudinal distance of front axle to vehicle CoG
a_c	longitudinal distance of cabin CoG to front axle
a_y	lateral acceleration
a_{yd}	maximum lateral acceleration
a_θ	longitudinal distance of tilt bearing to front axle
B_p	actuator damping coefficient
b	longitudinal distance of rear axle to vehicle CoG
b_θ	actuator tilt/displacement ratio
C_e	valve coefficient
C_s	suspension damping coefficient
$C_{\alpha f}$	front tyre slip stiffness coefficient
$C_{\alpha r}$	rear tyre slip stiffness coefficient
$C_{\theta f}$	front tyre camber coefficient
F_l	external load on actuators
F_y	lateral force on tyre
F_z	vertical force on tyre
g	gravitational acceleration
h_c	distance of cabin CoG from ground
h_r	distance of rear module CoG from ground
h_θ	distance of tilt bearing from ground
I_c	cabin roll inertia about CoG
I_r	rear module roll inertia about CoG
I_z	vehicle yaw inertia about CoG
K_{ayd}	lateral acceleration demand gain
$K_{\delta d}$	steer angle demand gain
$K_{\delta r}$	rear steer coefficient
K_c	pressure gain
K_q	flow gain

$K_{r\phi}$	roll bar stiffness
K_s	suspension spring stiffness
K_{xv}	spool displacement gain
$K_{\delta\theta}$	controller steering gain
$K_{\theta d}$	tilt angle demand gain
l	distance of tilt bearing to front tyre contact patch
l_c	see figure 7
L	wheel base
m	total vehicle mass
m_c	cabin mass
m_r	rear module mass
M_t	actuator piston mass
M_x	moment acting at the tilt bearing
q_c	flow into actuator due to oil compressibility
Q	actuator flow
Q_L	flow through the valve
R	corner radius
R_w	ratio of steering wheel to front wheel
R_y	lateral reaction force at tilt bearing
R_z	vertical reaction force at tilt bearing
r	yaw rate
T	rear wheel track
v	lateral velocity component
V	vehicle velocity
V	fluid volume in single actuator
V_t	total fluid volume in hydraulic system
x_p	actuator piston displacement
x_v	valve spool displacement
α_f	front tyre slip angle
α_r	rear tyre slip angle

α'	transient state slip angle
β	bulk modulus of hydraulic fluid
β_e	effective bulk modulus of hydraulic system
δ	resultant steer angle
δ_d	demand steer angle at the front wheel
δ_f	front steer angle
δ_w	driver steering angle input at the steering wheel
ΔF_z	load transfer across rear axle
ΔP_L	load pressure
γ	camber angle
μ	road surface friction coefficient
ϕ	roll angle of rear module
ψ	yaw angle
σ	tyre relaxation length
θ	relative tilt angle between cabin and rear module
θ_d	demand tilt angle
θ_{ss}	steady state tilt angle of cabin
ω	rotational speed
ξ	tilt axis inclination

References

[1] Anon. "Regulation (EC) No 443/2009 of the European Parliament and of the Council of 23 April 2009 setting emission performance standards for new passenger cars as part of the Community's integrated approach to reduce CO 2 emissions from light-duty vehicles (Text with EEA relevance)". Technical report, European Parliament, Council, 2009. Procedure number: COD(2007)0297.

[2] S-G. So and D. Karnopp. "Switching strategies for narrow ground vehicles with dual mode automatic tilt control". *Int. J. of Vehicle Design*, 18(5):518–532, 1997.

[3] S. So and D. Karnopp. "Active Dual Mode Tilt Control for Narrow Ground Vehicles". *Vehicle System Dynamics*, 27:19–36, 1997.

[4] D. Karnopp. "The Dynamics of Narrow, Automatically Tilted Commuter Vehicles". In *Proceedings of the 1997 EAEC Congress: Lightweight and small cars: the answer to future needs*, pages 13–19, 1997. Paper number 97A2KN08.

[5] B. Drew. "Tilt Control for a Narrow Track Vehicle". Obtained from: `http://www.bath.ac.uk/ptmc/research/docs/ proj_tilting_vehicle.pdf`.

[6] B. Drew. *Development of Active Tilt Control For A Three-Wheeled Vehicle*. PhD thesis, University of Bath, Bath, UK, 2006.

[7] C. van den Brink and H. Kroonen. "Dynamic Vehicle Control for Enclosed Narrow Vehicles". In *Proceedings of EAEC 6th European Congress: Lightweight and Small Cars—The Answer to Future Needs*, 2–4 July 1997. Paper number 97A2I22.

[8] C Van den Brink and H. Kroonen. "DVC — The banking technology driving the CARVER vehicle class". In *Proceedings of the 7th International Symposium on Advanced Vehicle Control (AVEC04)*, 13–20 Aug 2004.

[9] C. van den Brink and H. Kroonen. "Slender Comfort Vehicles: Offering the Best of Both Worlds". *AutoTechnology*, pages 56–59, 1/2004.

[10] J. C. Chiou and C. L. Chen. "Modeling and Verification of a Diamond-Shape Narrow-Tilting Vehicle". *IEEE/ASME Transactions on Mechatronics*, 13(6):678–691, 2008.

[11] J. C. Chiou, C. Y. Lin, C. L. Chen, and Chien C. P. "Tilting Motion Control in Narrow Tilting Vehicle Using Double-Loop PID Controller". In *Proceedings of the 7th Asian Control Conference*, pages 913–918, Hong Kong, China, 27–29 August 2009.

[12] S. Kidane, R. Rajamani, L. Alexander, P. Starr, and M. Donath. "Development and Experimental Evaluation of a Tilt Stability Control System for Narrow Commuter Vehicles". In *IEEE Transactions on Control Systems Technology*, volume 18, Nov 2010.

[13] S. Kidane, L. Alexander, R. Rajamani, P. Starr, and M. Donath. "A fundamental investigation of tilt control systems for commuter vehicles". *Vehicle System Dynamics*, 46(4):295–322, 2008.

[14] J. Berote. *Dynamics and Control of a Tilting Three Wheeled Vehicle*. PhD thesis, University of Bath, Bath, UK, 2010.

[15] J. Berote, A. Plummer, and J Darling. "Lateral Dynamics Optimisation of a Direct Tilt Controlled Narrow Vehicle". In *Proceedings of the 10th International Symposium on Advanced Vehicle Control (AVEC 2010)*, 22–26 Aug 2010.

[16] M. Barker, B. Drew, J. Darling, K. Edge, and G. W. Owen. "Steady-State Steering of a Tilting Three-Wheeled vehicle". *Vehicle System Dynamics*, 48(7):815–830, 2010.

[17] V. Cossalter. *"Motorcycle Dynamics 2nd Edition"*. LuLu (Self Publishing), 2006.

[18] H. B. Pacejka. *"Tyre and Vehicle Dynamics"*. Butterworth-Heinemann, 2002.

[19] H. S. Radt and W.F. Milliken. "Non-dimensionalizing Tyre Data for Vehicle Simulation". *Road Vehicle Handling*, 1983.

[20] W. F. Milliken and D. L. Milliken. *"Race Car Vehicle Dynamics"*. SAE, 1995.